IEEE Access
Multidisciplinary | Rapid Review | Open Access Journal

Received October 3, 2019, accepted October 18, 2019, date of publication October 28, 2019, date of current version November 7, 2019.

Digital Object Identifier 10.1109/ACCESS.2019.2949774

A Patch Based Denoising Method Using Deep Convolutional Neural Network for Seismic Image

YUSHU ZHANG, HONGBO LIN, YUE LI, AND HAITAO MA
Department of Information, College of Communication and Engineering, Jilin University, Changchun 130012, China

Corresponding author: Hongbo Lin (hblin@jlu.edu.cn)

This work was supported in part by the National Natural Science Foundation of China under Grant 41730422 and Grant 41774117, and in part by the National Natural Science Foundation of Jilin province of China under Grant 20170101167jc.

ABSTRACT The deep convolutional neural networks (CNNs) have been shown excellent performances for image denoising. However, the denoising CNN model trained with a specific noise level cannot deal with the images which have spatiotemporally variant random noise and low signal-to-noise ratio (SNR), such as seismic images. To this end, we propose a patch-based denoising CNN method, namely PDCNN. Specifically, we cluster the overlapping patches of noisy image into K classes where the image patches have close noise levels in each class, and then choose a suitable model for denoising the corresponding class from a series of well-trained CNN models. By embodying the structural statistics, we propose a CNN model selection criterion with a structural-dependent parameter. In contrast to the manual model selection process, the more accurate CNN model is chosen automatically and effectively. The capability of the PDCNN is demonstrated on synthetic and field seismic images. Experimental results show that the proposed method largely benefits from using multiple CNN models to jointly denoise, and leads to the satisfactory denoising performance in spatiotemporally variant seismic random noise reduction and structural signal preservation.

INDEX TERMS Convolutional neural networks (CNNs), clustering, patch, seismic image denoising, signal preservation, spatiotemporally variant random noise.

I. INTRODUCTION

Seismic exploration is the significant way for probing subsurface structures to explore oil and gas resources. One of main objects of the seismic signal processing is to accurately extract the effective seismic signals from observed noisy seismic images and then obtain information of complicated subsurface geological structures. However, acquired seismic data come with intensive interference and random noise generated from various noise origins such as winds and vehicle movements, causing the heavy degradation of the seismic data. Moreover, due to the acquisition way of the seismic data, the noise level usually varies spatiotemporally over seismic data, leading to the very low SNR in some local areas, which makes signal identification and extraction extremely difficult. Therefore, seismic image should be denoised to improve its quality, as well as preserving seismic signals. In the past decades, random noise reduction remains an active research topic in seismic signal processing. A huge amount of methods have been designed for seismic random noise reduction to meet the demands of the development in seismic exploration, such as wavelet transform-based denoising methods [1], [2], time-frequency peak filters [3]–[5], sparse representation [6], PDE-based diffusion filters [7], [8]. Although these denoising methods highly improve the quality of seismic images, the denoising performances still need to be improved under the condition of low SNR and spatiotemporally variant seismic random noise.

Recently, very impressive seismic denoising results have been achieved based on patch-based denoising methods. The nonlocal means algorithm (NLM) exploits a self-similarity to find the nonlocal similar patches for image denoising. The NLM has been applied in seismic random noise attenuation and effectively preserves the seismic energy across sharp discontinuities and curved events [9]. Another powerful example is the block matching and 3D collaborative filtering method (BM3D), which groups similar blocks by block matching and applies the collaborative filer to denoise the similar blocks in transform domain [10]. By using the local similarity of blocks, the BM3D algorithm achieves a benchmark denoising

The associate editor coordinating the review of this manuscript and approving it for publication was Huimin Lu.

This work is licensed under a Creative Commons Attribution 4.0 License. For more information, see http://creativecommons.org/licenses/by/4.0/

performance in preserving the details of seismic structural signals [11], [12]. For obtaining better sparse representations, dictionary learned from patches is used for effectively modeling seismic signals. Relative to the predefined dictionaries, such as curvelets, seislets, and shearlets, dictionary learning based methods have more powerful capacity to capture the structural features of seismic signals, and thereby improve denoising performance [13], [14].

Most recently, as computer hardware improves, it is feasible to train larger neural networks for learning more complex features intelligently. A typical example is the convolutional neural networks (CNNs). The deep CNNs have been widely applied in various fields and shown outstanding performances in object classification [15] and segmentation task [16]. Moreover, researchers began to apply the CNNs to solve the image restoration including deblurring [17], super-resolution [18], and denoising [19]–[21]. Zhang *et al.* [20], [21] proposed the denoising CNN models (DnCNNs) for image denoising. The denoising performance is superior to the state-of-the-art BM3D method. Furthermore, the CNNs also have been applied to seismic signal processing [22]–[24]. Yuan *et al.* [25] employed the CNN model for classifying time-space waveforms and picking first-breaks. The CNN-based model for 2-D image objection detection was also developed for identifying seismic events from seismic time series sets [26]. Zhao *et al.* [27] trained a denoising CNN model suitable for removing random noise in the desert area which has the characteristics of low frequency and non-Gaussianity. Zhu *et al.* [28] further utilized a deep neural network to remove a variety of seismic noise. By using transfer learning, Yu *et al.* [29] achieved a satisfied denoisng result of field seismic data based on the fact that the CNN model was trained by synthetic training set with fine tuned parameters. Consequently, the appropriate CNN denoising model is promising for the low SNR seismic images with spatiotemporally variant random noise.

Since the CNN model is a plain discriminative learning model, the single denoising CNN model trained with a specific noise level cannot obtain a satisfactory denoising performance for the noisy image with other noise level. Consequently, it is also found that only using a single CNN model is unable to achieve a promising denoising performance for the spatiotemporally variant random noise. Some improvements have been made for addressing this problem. The single CNN model named DnCNN-B, which is trained by a range of noise levels for blind Gaussian denoising in [21], can deal with spatiotemporally variant random noise, but it still has some trouble in well generalization for complicated real noisy images. In [30], a model named FFDNET is designed to handle the spatiotemporally variant random noise by adding a estimated noise level map as input of the CNN model. However, this method is practically not feasible for denoising seismic image due to the difficulty of estimating seismic noise level map and matching the model by trial and error. Unmatched CNN model may bring the distortion of the filtered signal and poor denoising capability. Therefore, in the areas with rich seismic features, more accurately and effectively choosing the CNN model is required for preserving signal while suppressing the spatiotemporally variant seismic random noise.

Motivated by patch-based denoising, we propose a patch-based denoising CNN method, namely PDCNN, which combines the patch clustering and multiple CNN models to remove the spatiotemporally variant random noise in seismic images. In the PDCNN, we decompose the noisy image into the overlapping patches, and then cluster the overlapping patches according to their estimated noise levels. In this way, one class only contains the patches with noise levels restricted in a small specific noise level range, and then a single CNN model is able to be selected for dealing with all patches in this class. Moreover, we train multiple CNN models associated with noise levels of the spatiotemporally variant random noise. The joint denoising strategy ensures the superior denoising ability of the PDCNN and effectiveness of removing the spatiotemporally variant random noise with sudden variation of noise level. Furthermore, a model selection criterion guided by structural statistics is proposed based on the relevance of the CNN model to the noise level range. As a consequent, the matched CNN model can be automatically and effectively chosen for each class, leading to outstanding denoising performance while preserving complicated morphology of seismic signals.

Note that the noise level of a filed seismic data is unavailable. In order to accurately estimate the noise variance of patches, we adopt a nonparametric statistical method in [31], which considers all eigenvalues of the covariance in redundant dimension rather than the smallest eigenvalue as the noise level estimation [32], [33]. As proved in [31], the adopted method is able to yield robust noise level estimation for the image patches with rich textures. The capability of the proposed method is demonstrated on both synthetic and field seismic images. Comparing with traditional seismic denoising methods and state-of-art denoising model, our method performs better in terms of signal preservation and spatiotemporally variant random noise reduction.

II. THEORY OF THE DENOISING CNN

In this section, we first introduce the denoising CNN model framework applied in our work, which is proposed in [20]. Then the updating process of parameters in the CNN model is also presented in detail.

A. THE CNN ARCHITECTURE USED FOR DENOISING

Based on the design of the CNN architecture and the training process, the learned CNN model attempts to predict the clean version from a corrupted image. Generally, the CNN model consists of the input layer, hidden layer, and output layer. The three kinds of layers of the CNN model applied in our work are composed by stack of operators which include the dilated convolution operator [34], the batch normalization (BN) operator [35], and the Rectified Linear Unit (ReLU) as the activation function.

The input layer contains a dilated convolution operator and a ReLU activation function. The hidden layer is made by the superposition of a dilated convolution operator, a BN operator, and a ReLU activation function in order, and the number of the hidden layer is changeable. The output layer only has a dilated convolution operator. With the aid of the three basic operators, the CNN model is constructed with multiple layers and different depths. Here the network depth is the same as the number of the layers. In general, the denoising ability of neural network will be effectively improved as the depth of network increases. But, too deep networks may fail to converge, along with increasing the burden of training due to excessive parameters. Hence, the depth of the network should be set appropriately based on the images to be processed.

The convolution operator captures the feature maps of the desired image during the training process. The deeper network yields lager receptive field, which means the context information in larger region of input image can be utilized by the convolution operator, playing an important role in the denoising performance. Consequently, for better trade-off between denoising performance and training efficiency, a proper size for the receptive field of the network needs to be considered. Here, the CNN model used in our work applies the dilated convolution operator to replace the ordinary convolution operator. The dilated convolution operator with a dilation factor s refers to the convolution operator only having 9 non-zeros parameters with fixed positions and s zeros between them, abbreviated as s-Dconv. The size of the s-Dconv is $(2s+1)\times(2s+1)$. Notably, when $s=1$, the 1-Dconv is the ordinary convolution operator with the size 3×3. The dilated convolutions can enlarge the receptive field without increasing the number of training parameters, which reduce the burden of training for considering the larger receptive field. For example, the desired receptive field size of 51×51 can be achieved by only 9 dilated convolution operators whose dilation factors are 1, 2, 3, 4, 5, 4, 3, 2, 1 in order. For the ordinary convolution, however, 25 operators are required to obtain the same receptive field size. Using the dilated convolution operator can reduce the number of training parameters as well as holding the denoising performance of network.

For the ReLU($\max(0, \mathbf{y})$), it is applied as the activation function which has been widely used in the deep learning frameworks. The ReLU function replaces the traditional sigmod function and reduces the vanishing gradient problem as speeding up the training. In addition to these two basic operators, the CNN model adopted in this paper also adds the BN operator. This operator described in detail in [35] is actually proposed to eliminate the Internal Covariate Shift problem which should not be neglected as the depth of network gradually increases. The BN layer also can support a faster convergence of training by using a higher learning rate. Moreover, using both the residual learning and the BN operator has been proved to make the model tend to obtain a better denoising performance during training [21]. Finally, the CNN framework by stacking the s-dilated convolution operator, the BN operator, and the ReLU activation function, has been proved to have the excellent denoising ability for single noise level [20]. In our work, we employ this model framework to train a series of CNN models with a wide range of noise levels.

B. THE UPDATING PROCESS OF THE CNN'S PARAMETERS

For image denoising, we need to recover a clean image $\mathbf{x}$ from a noisy observation $\mathbf{y}=\mathbf{x}+\mathbf{v}$, where $\mathbf{v}$ denotes additive noise assumed to be Gaussian. Most denoising CNNs based on the general training framework aim to learn the desired underlying mapping $H(\mathbf{y})$ to predict the clean image $\mathbf{x}$. Here, the CNN model based on residual learning is designed to learn the residual mapping $F(\mathbf{y},\Theta)$ to predict the residual noise $\mathbf{v}$, and $\mathbf{x}=\mathbf{y}-F(\mathbf{y},\Theta)$ is obtained as the denoised image [20]. Θ denotes all trainable parameters in the CNN model.

Generally, the CNN training learns all parameters Θ in the filters of the CNN model by minimizing the loss function, defined as the following

$$\ell(\Theta)=\frac{1}{2N}\sum_{i=1}^{N}\|F(\mathbf{y}_i,\Theta)-(\mathbf{y}_i-\mathbf{x}_i)\|^2 \tag{1}$$

where $\{((\mathbf{y}_i,\mathbf{x}_i)\}_{i=1}^{N}$ represents N noisy-clean training pairs. By using the classical backward propagation, the loss is propagated from the last layer to the first layer through the chain rule, thereby realizing the updating of various parameters. The parameter $\theta_l\in\Theta$ in the l-th layer is derived as:

$$\theta_l=\theta_l-\gamma(\partial\ell/\partial\theta_l) \tag{2}$$

where γ is the learning rate, and the derivative $\partial\ell/\partial\theta_l$ is acquired from the last layer to layer l by the chain rule.

As described above, the denoising performance of the CNN model is greatly affected by the training data, which is a common problem in the discriminative learning methods. When the noise level added to the training data is a single specific value, the trained CNN model has the outstanding denoising performance for the matching noise level, but has the limited denoising performance for other noise levels, thereby ill-suits the spatiotemporally variant random noise existed in the field seismic images.

III. THE PROPOSED PATCH-BASED DENOISING CNN METHOD

Based on the superior denoising ability of the single CNN model for its matching noise level, we propose a patch-based denoising CNN method (PDCNN) to remove the spatiotemporally variant random noise in seismic images, by combining the patch clustering and multiple denoising CNN models.

The flowchart of the proposed PDCNN algorithm has been shown in Figure 1. The PDCNN contains a training stage and a denoising stage. In the training process, we apply a 9-layer CNN model and train a set of models corresponding to multiple noise levels, using the residual learning framework. In the denoising stage, we have two steps including the patch

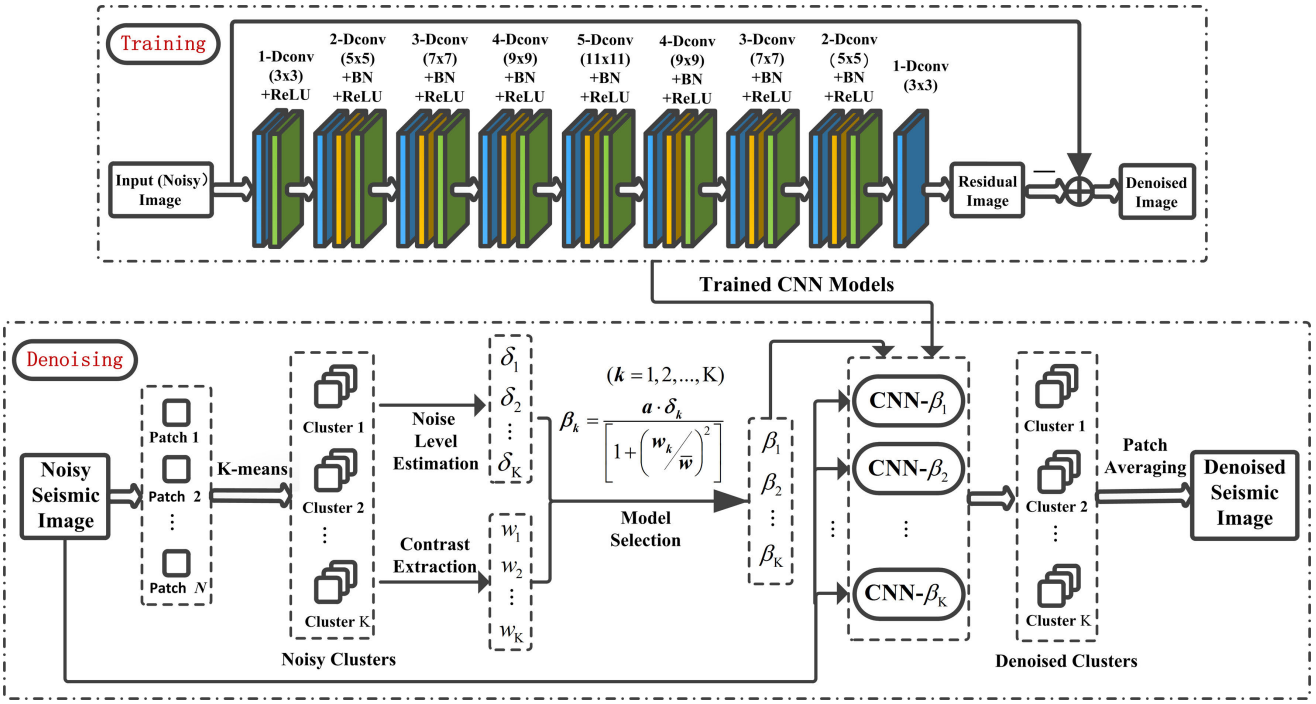

FIGURE 1. The flowchart of the proposed patch-based denoising CNN method.

clustering process and the denoising process with the multiple CNN models. Using the classical K-means clustering method, we obtain multiple clusters with small noise level ranges. In this way, each cluster contains the patches with similar noise levels and thus can be handled by a single CNN model trained by one specific noise level.

In addition, a model selection criterion related to the estimated noise level δ and the contrast w of each cluster is proposed to automatically and optimizedly select the final model CNN-β with the matching noise level β for each cluster, abbreviated as D_β. In order to give more consideration to signal preservation for those clusters containing rich structural textures, the contrast w is used to adjust the model selection process. It is worth to mention that the input of each CNN model is not multiple overlapping patches included in each cluster, but the overall noisy image, just for taking advantage of the receptive field of the network and not destroying the structures of the image. Each denoised version of noisy patches in cluster k is extracted from the output image of CNN model D_{β_k}, based on its original position in noisy image. Then, the final filtered result is obtained by averaging denoised overlapping patches.

A. THE PATCH CLUSTERING BASED ON THE NOISE LEVEL

The noise level of nonstationary seismic random noise changes significantly over seismic image. However, the noise level of small overlapping patch can be assumed as a constant, which makes it possible to select one CNN model to denoise such an image patch. With this in mind, we decompose the noisy image into overlapping image patches with the size $Q \times Q$. In our work, instead of separately matching the CNN model for each image patch, we cluster numerous patches according to their noise levels estimated by [31], and then select the desired CNN model to denoise each cluster, in order to simply and efficiently deal with large quantities of patches. For practical applications, the CNN model can slightly tolerate some noise level mismatch. In other words, the CNN model should be able to handle a small range of noise levels around its matching noise level. Therefore, the reasonable noise level range is critical to the patch clustering and model selection, which also determines the denoising performance of the proposed PDCNN algorithm.

We then analyze the feasibility of the noise level range on SNR improvement using a synthetic example. Three noisy images with normalized noise levels 0.16, 0.36, and 0.56 are respectively denoised by 40 CNN models $[\mathrm{D}_{0.02}, \mathrm{D}_{0.80}]$, where the subscript indicates the normalized noise level range [0.02, 0.80] with internal 0.02 used in training. As shown in Figure 2, the SNRs of the denoised results vary with respect to the training noise levels of the CNN models. Without doubt, the models $\mathrm{D}_{0.16}$, $\mathrm{D}_{0.36}$, and $\mathrm{D}_{0.56}$ obtain the best SNRs for three noisy images, respectively. If we set the 95% of the best SNR as the tolerable limit, models whose training noise levels selected from the range of [0.14, 0.20], [0.34, 0.40], and [0.54, 0.60] are the reasonable CNN models which work well for the three noisy images respectively. The results lead to a general phenomenon. For the noisy image with noise level B, the CNN models with training noise levels belonging to [B-0.02, B + 0.04] can be employed due to only the 5% attenuation from the best SNR of noise level B. Similarly, we can conclude that for one model D_β trained by single noise level β, the reasonable noise level range that D_β can handle

should be $[\beta - 0.04, \beta + 0.02]$ and the width of the range is about 0.06, for considering 5% attenuation from the best SNR of each noise level in the range $[\beta - 0.04, \beta + 0.02]$. It indicates that the width of noise level range for each cluster should be smaller than 0.06, and the corresponding noise level at the position of two thirds of noise level range in one cluster is feasible to match the CNN model.

In order to obtain better clusters, we utilize the aforementioned rule to infer the number K of the clusters and initial cluster centers for the K-means clustering algorithm. Let the noise level range of all overlapping image patches $[\delta_{min}, \delta_{max}]$, we first use the hard threshold to segment $[\delta_{min}, \delta_{max}]$ for obtaining the desired cluster number K and initial centers of the K-means clustering algorithm. First, all image patches are divided into K classes based on noise level according to the fixed width b. Setting the threshold $b \times k + \delta_{min}$ for the class k $(1 \leq k \leq K-1)$, the patch with noise level δ satisfying the condition: $b \times (k-1) + \delta_{min} \leq \delta < b \times k + \delta_{min}$ will be added to the class k. For the last class K, the condition is $b \times (K-1) + \delta_{min} \leq \delta \leq \delta_{max}$. Thus, we can obtain the number K of the clusters, and the means of noise levels in K classes are as the initial cluster centers of the K-means clustering. Here we consider that the noise level width of multiple clusters obtained by the K-means clustering is different, so we set the value of b less than 0.06. Finally, based on the classical K-means clustering, the obtained K clusters set can be written as $\mathrm{M} = \{\mathrm{M}_1, \mathrm{M}_2, \ldots, \mathrm{M}_K\}$. The cluster k $(1 \leq k \leq K)$ is denoted as $\mathrm{M}_k = \left\{\mathrm{M}_k^1, \mathrm{M}_k^2, \ldots, \mathrm{M}_k^R\right\}$, where R is the number of patches belonging to the cluster k.

B. THE CHOOSING OF THE OPTIMIZED CNN MODELS

To obtain the promising denoising performance in nonstationary seismic random noise attenuation and complex structural signal preservation, the suitable CNN model should be chosen for each cluster. The proposed model selection criterion considers three-fold.

First, the model selection depends on the estimated noise level from the overlapping patch. In practice, the mismatch between the estimated noise level and the real noise level is unavoidable. If the estimated one is lower than the real noise level, the random noise is unable to be completely removed, whereas the image details may be smoothed. In our work, instead of directly using the estimated noise level, we empirically select the CNN model slightly higher than the estimated noise level, for assuring the denoising performance. Second, the model selection should be automatic. For CNN denoising, manually selecting the CNN model is easy to introduce more errors, and becomes difficult for multiple clusters. Consequently, based on the estimated noise levels of all clusters, we consider automatically and optimizedly selecting the CNN models. Third, the texture information contents of all patches in each cluster should be taken into account. Since seismic images include complex structural textures, the CNN model just considering the denoising ability for random noise may smooth the seismic signals as well for those regions with rich features. So the PDCNN needs to select the model with a relatively lower training noise level for the detail preservation of the cluster which contains rich structural textures.

To this end, we propose a criterion for selecting the CNN model for each cluster guided by the structure statistic, which is presented as following:

$$\beta_k = \frac{a}{[1 + (\frac{w_k}{\overline{w}})^2]} \cdot \delta_k \quad (k = 1, 2, \ldots, K) \tag{3}$$

where $\delta_k (k = 1, 2, \ldots, K)$ is the estimated noise level of the k-th cluster and the corresponding β_k represents the matching noise level of the CNN model. The parameter a determines the upper limit of the model selection and generally takes a value bigger than 1.

For the whole texture contrast w_k of cluster k, $w_k = (1/R) \sum_{r=1}^{R} w_k^r$ $(1 \leq k \leq K)$ is the average of the contrasts of all patches in the cluster k, where w_k^r is the contrast of the patch M_k^r. $\overline{w} = (1/K) \sum_{k=1}^{K} w_k$ represents the mean of the whole texture contrasts of all clusters for normalizing w_k. The contrast w_k^r measures the local variations of the patch M_k^r and is calculated based on the gray-level cooccurrence matrix (GLCM) which is represented as [37]

$$w_k^r = \sum_i \sum_j (i-j)^2 C_k^r(i,j) \tag{4}$$

where the matrix C_k^r is the GLCM of the patch M_k^r and extracts the texture features by indicating the spatial distribution of gray level values at two pixels in a neighborhood of the patch M_k^r.

For the patch M_k^r with the size $Q \times Q$ whose gray level is scaled to m, its gray-level cooccurrence matrix C_k^r has the size $m \times m$, which is calculated by a probability function for measuring the probability of two pixels (i, j) occurring a given displacement vector $\vec{d} = (dx, dy)$ in M_k^r, defined as follows:

$$C_k^r(i,j) = \frac{u_{ij}}{(Q - dx)(Q - dy)} \tag{5}$$

where u_{ij} denotes the number of occurrence of the pixel values (i, j) posses at the displacement vector $\vec{d}$ in the patch. Practically, we apply a set of displacement vectors $\Delta = [\vec{d}_1 = (1, 0), \vec{d}_2 = (0, 1), \vec{d}_3 = (1, 1), \vec{d}_4 = (1, -1)]$. The final C_k^r is obtained by averaging four matrixes based on displacement vectors from Δ. Besides, in order to eliminate the noise interference for capturing the contrast of effective signals, Gaussian smoothing as the preprocessing is applied before computing the GLCM of each patch. In this way, the texture characteristics of all patches contained in each cluster entirely contribute to the selection of the CNN model for each cluster. Considering the size of the patch is smaller than the receptive field size of the network and the structural features of the whole image should not be destroyed, we take the whole noisy image as input for the CNN model of each cluster instead of using the patches in each cluster. As a result, K output images are obtained from the CNN models of K clusters. Then the denoised versions corresponding to noisy patches

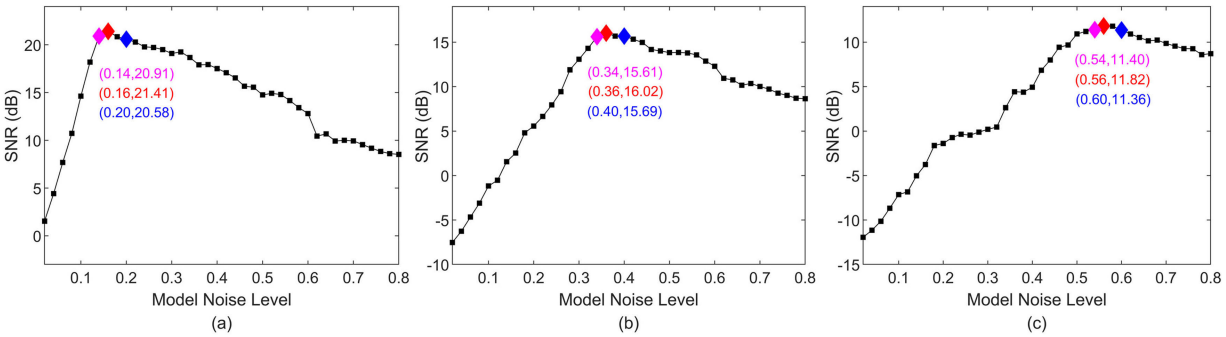

FIGURE 2. The SNR curves of three noisy images denoised by 40 CNN models trained by the specific normalized noise levels in the range [0.02,0.80]. (a) the noisy image with normalized noise level 0.16. (b) the noisy image with normalized noise level 0.36. (c) the noisy image with normalized noise level 0.56.

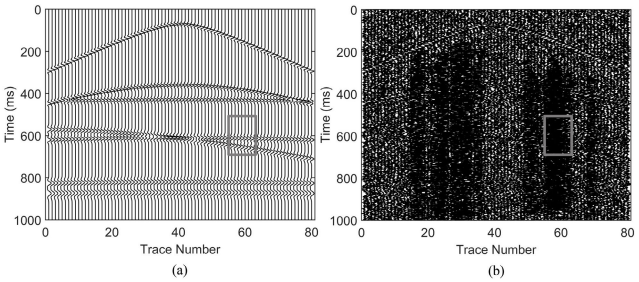

FIGURE 3. Synthetic noisy seismic image. (a) Ideal seismic image. (b) Noisy seismic image with spatiotemporal variant Gaussian noise (averaged SNR = −9.04 dB).

TABLE 1. Training times for different noise levels.

Noise Level	0.10	0.20	0.30	0.40	0.50	0.60	0.70	0.80
Training Time (h)	12.6	13.7	12.8	12.5	12.9	13.1	12.4	13.0

including in each cluster are extracted from the output image of each cluster. The final filtered image is reconstructed by averaging denoised overlapping patches.

IV. EXPERIMENT

In this section, we first give the training process, which includes building the training data sets suitable for the seismic image denoising and then training a series of CNN models with a wide noise level range. We apply the PDCNN based on a series of trained CNN models for the synthetic and field seismic images to verify its effectiveness.

A. TRAINING FOR DENOISING SEISMIC IMAGES

1) TRAINING DATA SETS

For seismic image denoising, we simulate the clean seismic image to construct training data by using the Ricker wavelet, which is defined as following

$$x(t) = A\left[1 - 2(\pi f_m(t - t_0))^2\right] \cdot exp(-(\pi f_m(t - t_0))^2) \quad (6)$$

where A is the amplitude, f_m is the dominant frequency and t_0 is the initial time. The synthetic seismic images contain multiple seismic events with different parameters f_m, t_0, and A. We set the dominant frequency f_m from 12 Hz to 63 Hz with the internal of 2 Hz while the amplitude A is chosen from [0.1 0.3 0.7 1]. The apparent velocity ranges from 600 m/s to 9000 m/s with the internal of 500 m/s. Finally, we obtain 82 synthetic clean seismic images where each seismic image is composed of 240 traces and 2000 samples per trace. We randomly select 75 images for training and 7 images as the test data. By adding the White Gaussian Noise (WGN) $\mathbf{v}$ with a fixed standard deviation σ to the clean seismic images, the noisy images are generated. The clean seismic images and the noisy seismic images are then cropped into image patches of size 60×60, and finally 128×1240 training pairs are obtained as one training set corresponding to noise level σ, similarly for the training sets of other noise levels. It is worth noting that the clean seismic images are normalized to $[-1, 1]$ by dividing their maximum value respectively before generating the noisy seismic images.

2) TRAINING

In our work, we set the normalized noise standard deviation σ changing from 0.02 to 0.80 with a step of 0.02 which covers the noise level range of the seismic images in our experiments. We generate 40 training data sets and train the corresponding 40 CNN models, respectively. In order to suit seismic image denoising, the depth of CNN model is empirically set to 9 based on the fact that the relatively larger size of the receptive field is beneficial for capturing the features of the seismic events with steep slopes. As a consequence, the whole network has the receptive field with the size of 51×51. Moreover, 64 convolution operators are utilized to generate 64 feature maps for every convolution layer.

During training, we use some common training strategies such as the Adam solver to optimize the updating process of parameters, for speeding up the mini-batch training and obtaining quick convergence rapidity [38]. We adjust the size of the mini-batch from small to large in multiples of 8 and best size of 128 is applied. Because using the residual learning and BN layer together makes the training converge steadily, the learning rate can be set as a larger value for speeding up training. We set the learning rate starting from 0.01 and

TABLE 2. Three criteria results of five methods on synthetic seismic images with different SNRs. The best results are highlighted.

Noisy Image	FK	Wavelet	BM3D	DnCNN-B	PDCNN
SNR_{avg}	SNR_{avg} / SNR_{local}	SNR_{avg} / SNR_{local}	SNR_{avg} / SNR_{local}	SNR_{avg} / SNR_{local}	SNR_{avg} / SNR_{local}
SNR_{local}	MSE / MSSIM	MSE / MSSIM	MSE / MSSIM	MSE / MSSIM	MSE / MSSIM
3.343	12.65 / 6.91	10.92 / 6.01	20.27 / **15.96**	19.67 / 12.88	**23.63** / 15.21
-3.61	9.34e-04 / 0.9919	0.0014 / 0.9903	1.61e-04 / 0.9988	1.85e-04 / 0.9985	**7.45e-05 / 0.9994**
-0.84	9.60 / 6.23	7.05 / 4.92	17.44 / 11.81	18.82 / 13.60	**21.42 / 19.51**
-5.85	0.0019 / 0.9825	0.0034 / 0.9769	3.10e-04 / 0.9975	2.25e-04 / 0.9981	**1.24e-04 / 0.9991**
-5.43	6.20 / 4.02	6.00 / 4.10	12.78 / 9.40	15.16 / 11.36	**18.12 / 17.52**
-9.40	0.0041 / 0.9599	0.0043 / 0.9594	9.06e-04 / 0.9921	8.34e-04 / 0.9941	**2.64e-04 / 0.9978**
-9.04	3.76 / 2.77	4.47 / 2.57	9.08 / 6.79	12.46 / 4.58	**15.94 / 18.36**
-12.46	0.0072 / 0.9236	0.0061 / 0.9297	0.0021 / 0.9823	9.76e-04 / 0.9913	**4.37e-04 / 0.9964**
-14.01	0.66 / -4.88	1.88 / 0.11	4.97 / 3.73	9.72 / 6.92	**10.68 / 9.79**
-19.54	0.0148 / 0.8464	0.0112 / 0.8589	0.0055 / 0.9457	0.0018 / 0.9846	**0.0015 / 0.9872**

exponentially reducing to 0.001 for fixed 100 epochs. In addition, it is found that training additional multiple epochs after the training error stops decreasing is slightly beneficial to obtain the model with a better denoising performance. In our work, when the training error stops decreasing, additional 10 epochs are adopted for training the CNN model. Alternatively, the training is terminated at maximum 100 epochs. The Matlab (R2018a) with MatConvNet package on an Nvidia GeForce GTX 1080Ti GPU is used to train the CNN models. We find that the training generally is terminated within about 70 epochs for different noise levels. Table 1 gives the training times of 8 noise levels with 0.1:0.1:0.8. The training times of 40 noise levels are different and they slightly fluctuate near 12.5 hours.

B. DENOISING

In order to evaluate the performance of the proposed method in removing spatiotemporally variant random noise and preserving seismic signal, we employ the proposed PDCNN on the synthetic and field seismic images. Results are compared with four algorithms including the FK filter, Wavelet-based denoising method, BM3D method, and the DnCNN-B model. For quantitative evaluation of denoising performance, we further calculate the SNR, mean squared error (MSE), and mean structure similarity (MSSIM) [39] corresponding to the synthetic image. The SNR and MSE are computed by

$$\mathrm{SNR(dB)} = 10\log_{10}\frac{\sum_{i=1}^{L}|z_i|^2}{\sum_{i=1}^{L}|z_i - q_i|^2} \tag{7}$$

$$\mathrm{MSE} = \frac{1}{L}\sum_{i=1}^{L}(z_i - q_i)^2 \tag{8}$$

where z is the ideal signal, q is the denoised signal, and L is the length of the signal. The MSSIM is also used to measure the mean structure similarity between the ideal data $\mathbf{X}$ and the filtered data $\mathbf{Y}$, which is defined as

$$\mathrm{MSSIM}(\mathbf{X}, \mathbf{Y}) = \frac{1}{J}\sum_{j=1}^{J}\mathrm{SSIM}(\mathbf{x}_j, \mathbf{y}_j) \tag{9}$$

where $\mathbf{x}_j$ and $\mathbf{y}_j$ are the image contents in the j-th local window. J is the number of local windows of the data. The structure similarity (SSIM) between $\mathbf{x}_j$ and $\mathbf{y}_j$ is calculated as

$$\mathrm{SSIM}(\mathbf{x}_j, \mathbf{y}_j) = \frac{(2\mu_x\mu_y + C_1)\times(\sigma_{xy} + C_2)}{(\mu_x^2 + \mu_y^2 + C_1)\times(\sigma_x\sigma_y + C_2)} \tag{10}$$

where μ_x and σ_x are the mean intensity and standard deviation of $\mathbf{x}_j$. μ_y and σ_y are the mean intensity and standard deviation of $\mathbf{y}_j$. σ_{xy} is the covariance of $\mathbf{x}_j$ and $\mathbf{y}_j$. C_1 and C_2 are the constants in order to maintain stability.

1) SYNTHETIC SEISMIC DATA

To investigate the validity of the proposed method, we apply our method to the synthetic seismic image which consists of seven seismic events with the dominant frequencies of 50 Hz, 45 Hz, 38 Hz, 32 Hz, 30 Hz, 25 Hz, and 20 Hz shown in Figure 3(a). The noisy seismic data are generated by adding the WGN with spatiotemporally variant levels. The noisy seismic image shown in Figure 3(b) has the average SNR of −9.04dB.

We employ the FK filter, Wavelet-based denoising method, BM3D, DnCNN-B, and the proposed PDCNN on the noisy image. Figure 4(a), (c), (e), (g), and (i) illustrate the filtered results using five denoising methods. The difference images between five denoised seismic images and noise-free seismic image are shown in Figure 4(b), (d), (f), (h), and (j). From Figure 4(a), it is observed that the FK filter can remove a certain amount of spatiotemporally variant random noise and partly reveal the seismic events. However, the residual noise and signal loss are clearly observed in the difference image shown in Figure 4(b). The Wavelet method shows a certain capacity of suppressing intensive random noise and results in a clean background in Figure 4(c). But,

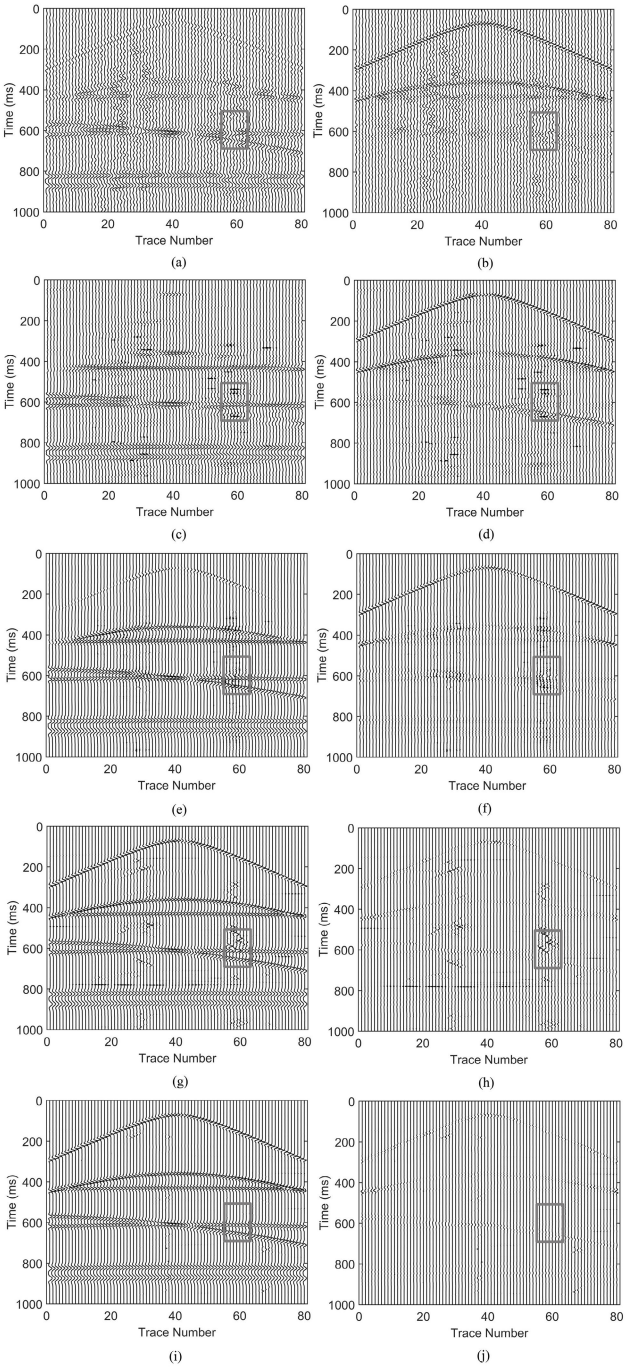

FIGURE 4. Denoising results of a synthetic seismic record with spatiotemporal variant Gaussian noise using five methods. (a) Result of the FK filter. (b) The difference of the pure seismic image and result of FK filter. (c) Result of the Wavelet-based denoising method. (d) The difference of the pure seismic image and result of Wavelet-based denoising method. (e) Result of the BM3D method. (f) The difference of the pure seismic image and result of BM3D method. (g) Result of the DnCNN-B method. (h) The difference of the pure seismic image and result of DnCNN-B. (i) Result of the PDCNN method. (j) The difference of the pure seismic image and result of PDCNN method.

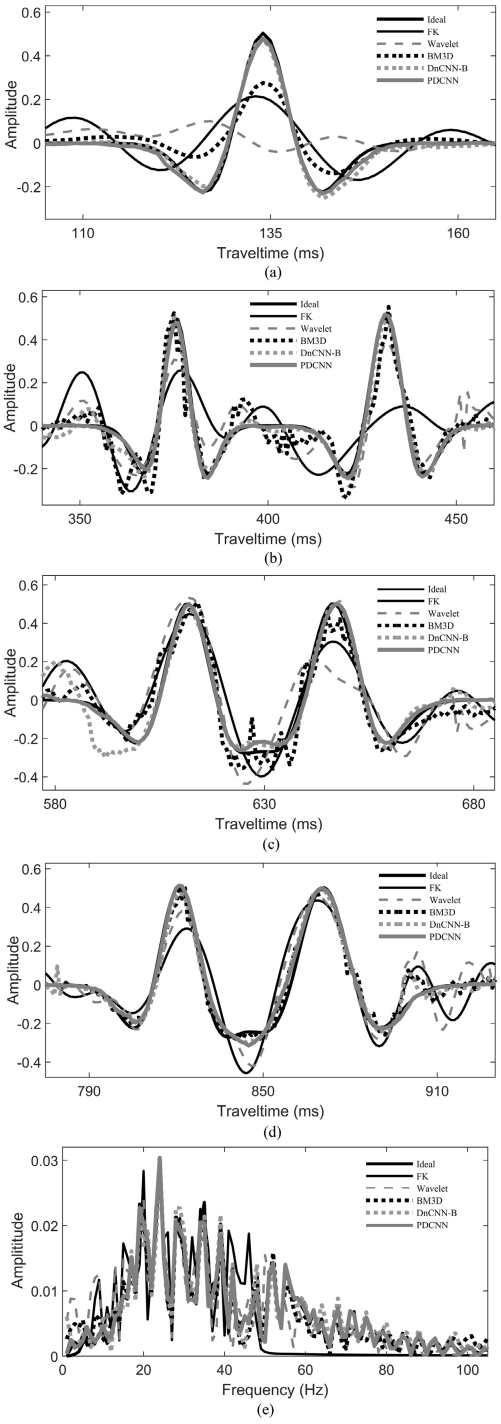

FIGURE 5. Single-trace waveforms and amplitude spectrum comparison denoisied by five methods (the 56th traces of Figure 4). (a) First wave of trace 56 (50HZ). (b) Second and third waves of trace 56 (45Hz and 38Hz). (c) Fourth and fifth waves of trace 56 (32Hz and 30H). (d) Sixth and seventh waves of trace 56 (25Hz and 20Hz). (e) Amplitude spectrum of the signal in the 56th trace of Figure 4.

the Wavelet method excessively smoothes effective seismic events, especially for the first and second seismic events with large slopes, due to its poor ability of describing the curved features of seismic events. In contrast, the BM3D, DnCNN-B, and our method do better in random noise attenuation than the FK filter and Wavelet method. Moreover, the DnCNN-B and our method have better performances in preserving signals than the BM3D method. The seismic events recovered by the DnCNN-B and the proposed PDCNN

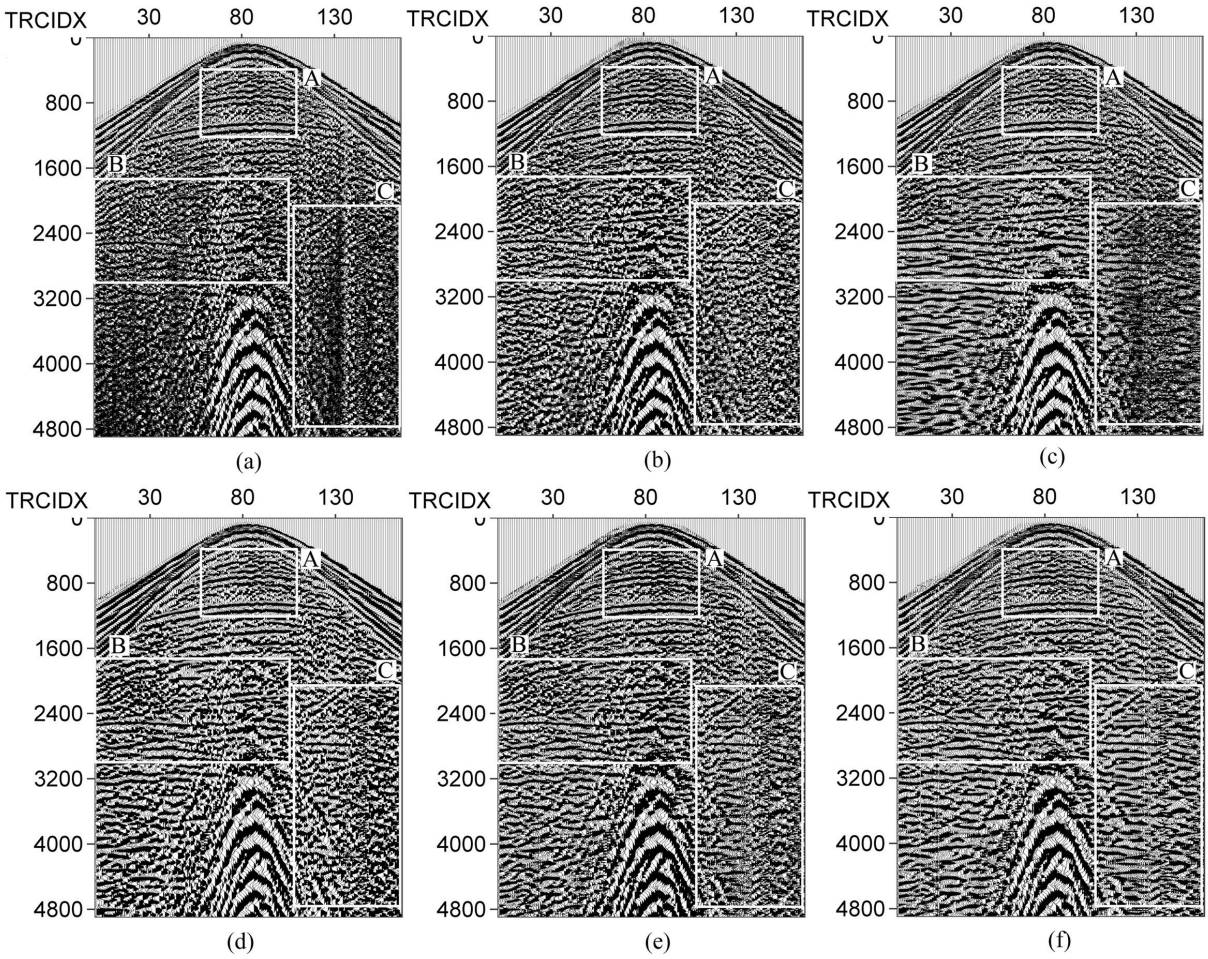

FIGURE 6. Filtered results of a real seismic record by applying five different mehods. (a) Noisy record. (b) Denoised by the FK filter. (c) Denoised by the Wavelet-based denoising method. (d) Denoised by the BM3D method. (e) Denoised by the DnCNN-B method. (f) Denoised by the PDCNN method.

both become continuous and complete, which also can be verified by the difference images in Figure 4(h) and (j). In comparison with the DnCNN-B, our method obtains the cleaner background in the filtered seismic image. The spatiotemporally variant random noise is almost reduced and cannot be observed in Figure 4(i) using the PDCNN while some random noise is visible in Figure 4(g) by applying the DnCNN-B. The experimental results demonstrate that our method outperforms the other four denoising methods in suppression of spatiotemporally variant seismic random noise and signal preservation.

Additionally, in order to emphasize the efficiency of the proposed method, we compare the denoising performances of the 56th seismic trace of five filtered results in time and frequency domain. As illustrated in Figure 5(a)-(d), the filtered signals of CNN-based denoising methods (DnCNN-B and PDCNN) are closer to the ideal signal than the other three methods, while the PDCNN makes the recovered signals more complete and symmetric than the DnCNN-B. In the aspect of noise suppression, the proposed PDCNN is able to completely remove out the spatiotemporally variant random noise, while some intensive residual noise is visible by applying the other four methods. In addition, the PDCNN also outperforms the other four methods in the frequency domain shown in the Figure 5(e). Consequently, the proposed method is more adaptable to reduce spatiotemporally variant random noise in seismic image than the other four methods.

Next, we give quantitative comparisons of five denoising methods in terms of aforementioned SNR, MSE, and MSSIM listed in the Table 2, and the best results are highlighted in bold. In comparison to the other four methods, the PDCNN provides the best performance with the highest SNR_{avg}, refer to the average SNR, lowest MSE, and highest MSSIM. Additionally, the SNR for the local area as SNR_{local} is also computed, from 56 to 62 traces with the time range of 500-700 ms marked in Figure 3 and 4, and the SNR_{local} of noisy seismic image reaches -12.46dB. Since this selected area contains rich signals and strong random noise with almost maximum intensity, the PDCNN has more improvement in SNR_{local} of 30.82 dB than SNR_{avg} of 24.98 dB, which further verifies its signal preserving ability and denoising ability for strong random noise.

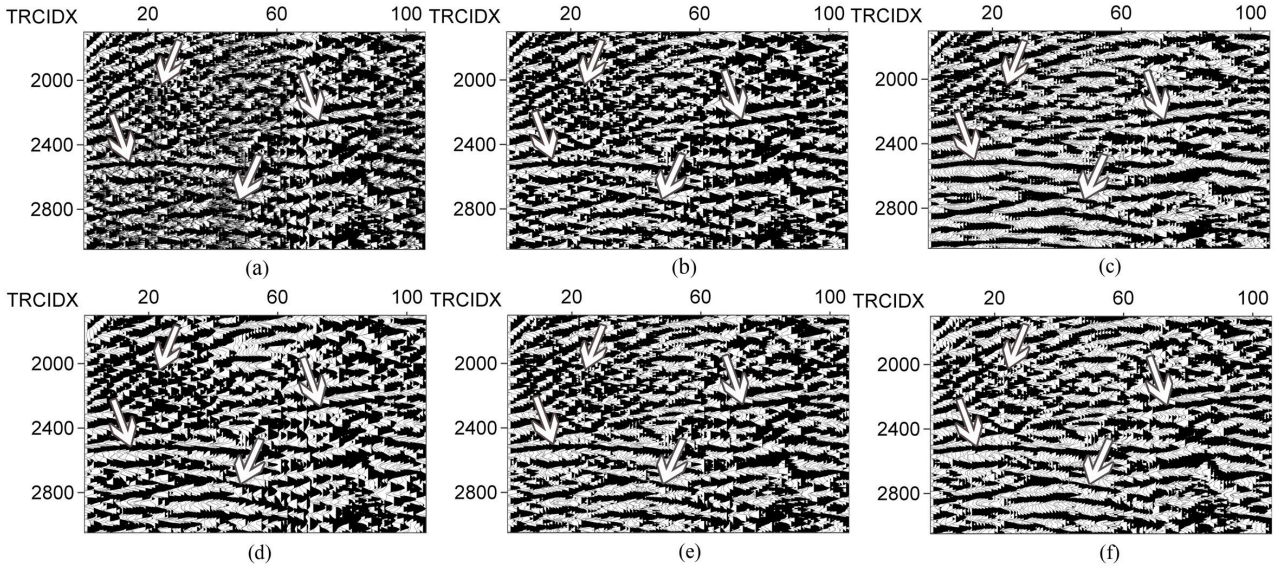

FIGURE 7. Denoised Performance comparison of five methods in the selected region B. (a) Noisy record. (b) Denoised by the FK filter. (c) Denoised by the Wavelet-based denoising method. (d) Denoised by the BM3D method. (e) Denoised by the DnCNN-B method. (f) Denoised by the PDCNN method.

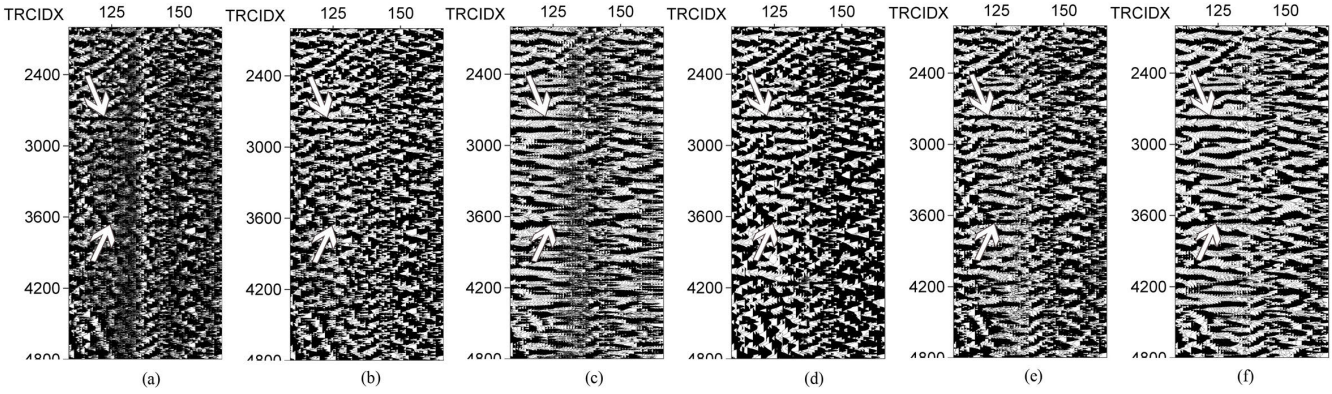

FIGURE 8. Denoised Performance comparison of five methods in the selected region C. (a) Noisy record. (b) Denoised by the FK filter. (c) Denoised by the Wavelet-based denoising method. (d) Denoised by the BM3D method. (e) Denoised by the DnCNN-B method. (f) Denoised by the PDCNN method.

To illustrate the efficacy of our approach in case of different SNRs, we change the average SNRs and compute the denoised results by applying the five algorithms. Table 2 presents the comparison of the performance indexes of the results. The proposed PDCNN method almost has the best results in SNR_{avg}, SNR_{local}, MSE, and MSSIM on different average SNRs experiments, especially for low SNRs, which indicates that the PDCNN is more suitable for removing spatiotemporally variant random noise even at low SNR, compared with the other four denoising approaches.

2) FIELD SEISMIC DATA

This part is designed to assess the effects of the proposed PDCNN on the field common-shot-point seismic record shown in Figure 6(a). The selected 165-trace prestack seismic data are collected from a forest belt in China and contain 4900 samples in each trace with the sampling frequency of 1 K Hz. As can be seen from Figure 6(a), the seismic data are seriously corrupted by the random noise with spatiotemporally variant noise levels. We marked three typical areas by rectangles with labels of A, B, and C. The seismic signals in the area A are relatively weak and not continuous due to noise interference. In the area B, we can observe that strong variant random noise makes reflection events distorted. The most intensive random noise exists in the area C, where the seismic events are almost unable to be identified.

The FK filter, Wavelet-based denoising method, BM3D, DnCNN-B, and PDCNN are applied to this noisy record and corresponding results are represented in Figure 6(b)-(f). As illustrated in Figure 6(b), (d), and (e) provided by the FK, BM3D, and DnCNN-B respectively, plenty of random noise has been reduced by the three methods, while the DnCNN-B has the best denoising performance. The Wavelet method can remove low intensity random noise, but is unable to reduce

some strong field seismic random noise, especially those in domain C of Figure 6(c). Figure 6(f) indicates that using our proposed technique leads to much better image in term of removing random noise and preserving signal details than the other four methods. The seismic signals are effectively revealed and become smoother and more continuous, even in the area C.

For a better visualization and comparison, we next zoom in on two typical areas (domain B and C) from the noisy seismic image and denoised results. The domain B is from 1 to 105 traces with the time range of 1700-3050 ms, shown in Figure 7. As can be seen in domain B, the results provided by the FK filter and the BM3D do worse than other three approaches in reducing random noise. The DnCNN-B removes a majority of random noise, but is inferior to the Wavelet-based denoising method and the proposed PDCNN, which both achieve the good denoising performance with a trivial difference (see arrows in Figure 7). The domain C from 110 to 165 traces with the time range of 2000-4800 ms is illustrated in Figure 8. Note that the FK filter and the BM3D both show that there is still residual noise in the entire area. For the Wavelet-based denoising method, the ability for removing intensive random noise is weaker than reducing low intensity noise. For the DnCNN-B, it can eliminate some spatiotemporally variant random noise and the denoising ability is stronger than the FK filter, Wavelet-based denoising method, and BM3D, but accompanying some strong random noise residual. Comparing to the other four methods, the proposed PDCNN not only effectively removes the spatiotemporally variant random noise whether it is weak or strong, but also recovers the seismic events clearly (see arrows in Figure 8). In summary, the experimental results on field seismic image demonstrate that the denoising capacity and signal preservation of the proposed PDCNN are superior to the other four methods.

V. CONCLUSION

In this paper, the PDCNN is proposed to suppress the spatiotemporally variant seismic random noise. Its critical point lies in patches clustering and joint denoising with multiple CNN models to handle all the noise levels existing in the spatiotemporally variant random noise. We show the feasibility that the PDCNN automatically and optimizedly selects the CNN models for removing the seismic random noise with spatiotemporally variant levels. Meanwhile, effective seismic events with complex features are preserved well and their continuity is also enhanced. The experiments of the synthetic and field seismic images finally validate the excellent performance of our proposed PDCNN, which also illustrate that the CNN-based methods have extensive application prospects in seismic image denoising.

REFERENCES

[1] S. Gaci, "The use of wavelet-b.ased denoising techniques to enhance the first-arrival picking on seismic traces," *IEEE Trans. Geosci. Remote Sens.*, vol. 52, no. 8, pp. 4558–4563, Aug. 2014.

[2] R. Anvari, M. A. N. Siahsar, S. Gholtashi, A. R. Kahoo, and M. Mohammadi, "Seismic random noise attenuation using synchrosqueezed wavelet transform and low-rank signal matrix approximation," *IEEE Trans. Geosci. Remote Sens.*, vol. 55, no. 11, pp. 6574–6581, Nov. 2017.

[3] Y. Tian, Y. Li, and B. Yang, "Variable-eccentricity hyperbolic-trace TFPF for seismic random noise attenuation," *IEEE Trans. Geosci. Remote Sens.*, vol. 52, no. 10, pp. 6449–6458, Oct. 2014.

[4] H. Lin, Y. Li, H. Ma, B. Yang, and J. Dai, "Matching-pursuit-based spatial-trace time-frequency peak filtering for seismic random noise attenuation," *IEEE Geosci. Remote Sens. Lett.*, vol. 12, no. 2, pp. 394–398, Feb. 2015.

[5] H. Lin, Y. Li, B. Yang, H. Ma, and C. Zhang, "Seismic random noise elimination by adaptive time-frequency peak filtering," *IEEE Geosci. Remote Sens. Lett.*, vol. 11, no. 1, pp. 337–341, Jan. 2014.

[6] P. Turquais, E. G. Asgedom, and W. Söllner, "A method of combining coherence-constrained sparse coding and dictionary learning for denoising," *Geophysics*, vol. 82, no. 3, pp. 137–148, Feb. 2017.

[7] Q. Zhou, J. Gao, Z. Wang, and K. Li, "Adaptive variable time fractional anisotropic diffusion filtering for seismic data noise attenuation," *IEEE Trans. Geosci. Remote Sens.*, vol. 54, no. 4, pp. 1905–1917, Apr. 2016.

[8] Y. Zhang and H. Lin, "The adaptive complex shock diffusion for seismic random noise attenuation," in *Proc. IEEE Conf. Signal Inf. Process. (GlobalSIP)*, Nov. 2017, pp. 333–337.

[9] D. Bonar and M. Sacchi, "Denoising seismic data using the nonlocal means algorithm," *Geophysics*, vol. 77, no. 1, pp. A5–A8, 2012.

[10] K. Dabov, A. Foi, V. Katkovnik, and K. Egiazarian, "Image denoising by sparse 3-D transform-domain collaborative filtering," *IEEE Trans. Image Process.*, vol. 16, no. 8, pp. 2080–2095, Aug. 2007.

[11] H. Wang, S. Cao, K. K. Jiang, H. Wang, and Q. C. Zhang, "Seismic data denoising for complex structure using BM3D and local similarity," *J. Appl. Geophys.*, vol. 170, pp. 1–9, Nov. 2019.

[12] C. Zhang, M. van der Baan, Y. Li, and X. C. Xu, "Microseismic and seismic denoising using block matching and 3-D collaborative filtering," in *Proc. 87th Annu. Meeting SEG Int. Expo.*, Sep. 2017, pp. 5022–5026.

[13] H. B. Lin, H. R. Xi, Y. Li, and H. T. Ma, "Nonstationary seismic random noise attenuation by EPLL," in *Proc. IEEE Conf. Image Process.*, Oct. 2018, pp. 1103–1107.

[14] L. Liu, J. W. Ma, and G. Plonk, "Sparse graph-regularized dictionary learning for suppressing random seismic noise," *Geophysics*, vol. 83, no. 3, pp. v215–v231, May-Jun. 2018.

[15] A. Krizhevsky, I. Sutskever, and G. E. Hinton, "Imagenet classification with deep convolutional neural networks," in *Proc. Adv. Neural Inf. Process. Syst.*, 2012, pp. 1097–1105.

[16] L.-C. Chen, G. Papandreou, I. Kokkinos, K. Murphy, and A. L. Yuille, "DeepLab: Semantic image segmentation with deep convolutional nets, atrous convolution, and fully connected CRFs," *IEEE Trans. Pattern Anal. Mach. Intell.*, vol. 40, no. 4, pp. 834–848, Apr. 2018.

[17] C. Min, G. Wen, B. Li, and F. Fan, "Blind deblurring via a novel recursive deep CNN improved by wavelet transform," *IEEE Access*, vol. 6, pp. 69242–69252, 2018.

[18] Y. Zhang, L. Sun, C. Yan, X. Ji, and Q. Dai, "Adaptive residual networks for high-quality image restoration," *IEEE Trans. Image Process.*, vol. 27, no. 7, pp. 3150–3163, Jul. 2018.

[19] W. Yang, H. Zhang, J. Yang, J. Wu, X. Yin, Y. Chen, H. Shu, L. Luo, G. Coatrieux, Z. Gui, and Q. Feng, "Improving low-dose CT image using residual convolutional network," *IEEE Access*, vol. 5, pp. 24698–24705, 2017.

[20] K. Zhang, W. Zuo, S. Gu, and L. Zhang, "Learning deep CNN denoiser prior for image restoration," in *Proc. IEEE Conf. Comput. Vis. Pattern Recognit.*, Jul. 2017, pp. 2808–2817.

[21] K. Zhang, W. Zuo, Y. Chen, D. Meng, and L. Zhang, "Beyond a Gaussian Denoiser: Residual learning of deep CNN for image denoising," *IEEE Trans. Image Process.*, vol. 26, no. 7, pp. 3142–3155, Jul. 2017.

[22] S. M. Mousavi, W. Zhu, Y. Sheng, and G. C. Beroza, "CRED: A deep residual network of convolutional and recurrent units for earthquake signal detection," *Sci. Rep.*, vol. 9, no. 1, p. 10267, Jul. 2019.

[23] Z. E. Ross, M.-A. Meier, and E. Hauksson, "P wave arrival picking and first-motion polarity determination with deep learning," *J. Geophys. Res.*, vol. 123, pp. 5120–5129, Jun. 2018.

[24] J. Zheng, J. Lu, S. Peng, and T. Jiang, "An automatic Microseismic or acoustic emission arrival identification scheme with deep recurrent neural networks," *Geophys. J. Int.*, vol. 212, pp. 1389–1397, Feb. 2018.

[25] S. Yuan, J. Liu, S. Wang, T. Wang, and P. Shi, "Seismic waveform classification and first-break picking using convolution neural networks," *IEEE Geosci. Remote Sens. Lett.*, vol. 15, no. 2, pp. 272–276, Feb. 2018.
[26] Y. Wu, Y. Lin, Z. Zhou, D. C. Bolton, J. Liu, and P. Johnson, "DeepDetect: A cascaded region-based densely connected network for seismic event detection," *IEEE Trans. Geosci. Remote Sens.*, vol. 57, no. 1, pp. 62–75, Jan. 2019.
[27] Y. Zhao, Y. Li, X. Dong, and B. Yang, "Low-frequency noise suppression method based on improved DnCNN in desert seismic data," *IEEE Geosci. Remote Sens. Lett.*, vol. 16, no. 5, pp. 811–815, May 2019.
[28] W. Zhu, A. C. Bovik, S. Mostafa Mousavi, and G. C. Beroza, "Seismic signal denoising and decomposition using deep neural networks," *IEEE Trans. Geosci. Remote Sens.*, to be published.
[29] S. Yu, J. Ma, and W. Wang, "Deep learning for denoising," *Geophysics*, vol. 84, no. 6, pp. v333–v350, Oct. 2019.
[30] K. Zhang, W. Zuo, and L. Zhang, "FFDNet: Toward a fast and flexible solution for CNN-based image denoising," *IEEE Trans. Image Process.*, vol. 27, no. 9, pp. 4608–4622, Sep. 2018.
[31] G. Chen, F. Zhu, and P. A. Heng, "An efficient statistical method for image noise level estimation," in *Proc. IEEE Conf. Comput. Vis.*, Dec. 2015, pp. 477–485.
[32] X. Liu, M. Tanaka, and M. Okutomi, "Single-image noise level estimation for blind denoising," *IEEE Trans. Image Process.*, vol. 22, no. 12, pp. 5226–5237, Dec. 2013.
[33] S. Pyatykh, J. Hesser, and L. Zheng, "Image noise level estimation by principal component analysis," *IEEE Trans. Image Process.*, vol. 22, no. 2, pp. 687–699, Feb. 2013.
[34] F. Yu and V. Koltun, "Multi-scale context aggregation by dilated convolutions," in *Proc. Int. Conf. Learn. Represent.*, 2016.
[35] S. Ioffe and C. Szegedy, "Batch normalization: Accelerating deep network training by reducing internal covariate shift," in *Proc. Int. Conf. Mach. Learn.*, 2015, pp. 448–456.
[36] K. He, X. Zhang, S. Ren, and J. Sun, "Deep residual learning for image recognition," in *Proc. IEEE Conf. Comput. Vis. Pattern Recognit.*, Jun. 2016, pp. 770–778.
[37] M. Bevk and I. Kononenko, "A statistical approach to texture description of medical images: A preliminary study," in *Proc. 15th IEEE Symp. Comput.-Based Med. Syst. (CBMS)*, Maribor, Slovenia, Jun. 2002, pp. 239–244.
[38] D. Kingma and J. Ba, "Adam: A method for stochastic optimization," in *Proc. Int. Conf. Learn. Represent.*, 2015.
[39] Z. Wang, A. C. Bovik, H. R. Sheikh, and E. P. Simoncelli, "Image quality assessment: From error visibility to structural similarity," *IEEE Trans. Image Process.*, vol. 13, no. 4, pp. 600–612, Apr. 2004.

YUSHU ZHANG received the B.S. degree in biomedical engineering from Jilin University, Changchun, China, in 2016, where she is currently pursuing the Ph.D. degree, under the supervision of Prof. H. Lin. Her current research interests include complex diffusion, deep learning, and seismic image denoising.

HONGBO LIN received the B.S. degree in automatic control from the Jilin University of Technology, Changchun, China, in 1996, and the Ph.D. degree in geophysics from Jilin University, in 2007. She is currently a Professor of information and communication system with the Department of Information Engineering, Jilin University. Her current research interests include weak signal extraction, time-frequency analysis, seismic signal processing, and multidimensional signal processing.

YUE LI received the B.S. degree in automatic control from the University of Technology, Changchun, China, in 1982, and the Ph.D. degree in earthscope from Jilin University, Changchun, in 2001. She is currently a Professor of communication and information system with the Department of Communication Engineering, Jilin University. She has authored more than 100 articles on weak signal detection, real-time signal processing, nonlinear dynamic systems, random signal processing, Radon-Wigner transform, particle filter, time-frequency analysis, weak seismic information extraction, and medical signal processing, and coauthored two books, *Methodology of Periodic Oscillator Detection* and *Periodic Oscillator System and Detection*.

HAITAO MA received the B.S. degree in optoelectronic technology from the Jilin University of Technology, Changchun, China, in 1991, and the Ph.D. degree from the Changchun Institute of Optics, Chinese Academy of Sciences, China, in 2004. He is currently a Professor of information and communication system with the Department of Information Engineering, Jilin University. His current research interests include weak signal detection, signal analysis systems, and optical signal processing.